Pure Appl. Geophys. 171 (2014), 3143–3157

DOI 10.1007/s00024-014-0787-x

Pure and Applied Geophysics

Fault Wear by Damage Evolution During Steady-State Slip

Vladimir Lyakhovsky,[1] Amir Sagy,[1] Yuval Boneh,[2] and Ze'ev Reches[3]

Abstract—Slip along faults generates wear products such as gouge layers and cataclasite zones that range in thickness from sub-millimeter to tens of meters. The properties of these zones apparently control fault strength and slip stability. Here we present a new model of wear in a three-body configuration that utilizes the damage rheology approach and considers the process as a micro-fracturing or damage front propagating from the gouge zone into the solid rock. The derivations for steady-state conditions lead to a scaling relation for the damage front velocity considered as the wear-rate. The model predicts that the wear-rate is a function of the shear-stress and may vanish when the shear-stress drops below the microfracturing strength of the fault host rock. The simulated results successfully fit the measured friction and wear during shear experiments along faults made of carbonate and tonalite. The model is also valid for relatively large confining pressures, small damage-induced change of the bulk modulus and significant degradation of the shear modulus, which are assumed for seismogenic zones of earthquake faults. The presented formulation indicates that wear dynamics in brittle materials in general and in natural faults in particular can be understood by the concept of a "propagating damage front" and the evolution of a third-body layer.

Key words: Fault wear, Wear-rate, Friction, Damage rheology.

1. Introduction

Wear is a fundamental process in shearing surfaces that was studied experimentally and theoretically, especially for engineering materials (Archard 1953; Archard and Hirch 1956; Queener *et al*. 1965; Levy and Jee 1988; Kato and Adachi 2000). However, the mechanics of the process in a three-body configuration is still poorly understood. The Archard model for wear between sliding solid blocks states that the wear volume linearly increases with applied normal stress (Archard 1953). This prediction is not consistent with recent experimental results of shearing rock faults demonstrating that wear-rates at steady-state conditions strongly depend on slip velocity.

Slip along faults in the upper crust is always associated with wear of the shearing rock blocks (Power *et al*. 1988; Scholz 2002), as evident by slickenside striations (Petit 1987) and gouge zones (Engelder 1974; Sibson 1977; Chester and Logan 1987). The wear processes strongly affect the fault structure. First, the plucking and crushing of fault surface asperities during shear (Fig. 1a) (Wang and Scholz 1994) modifies the geometry of the fault slip surfaces (Sagy and Brodsky 2009). Second, the wear leads to the establishment of gouge and cataclasite zones (Fig. 1b) that range in thickness from sub-millimeter to tens of meters (Katz *et al*. 2003; Wilson *et al*. 2005; Shipton *et al*. 2006; Wibberley *et al*. 2008). Experimental works showed that a gouge zone may be established after short slip distances of just a few centimeters (Boneh 2012). Thus, the existence of a gouge-zone transforms the fault slip from a "two-body" mode, in which the shearing occurs at direct contacts between asperities (Fig. 1a), into a "three-body" mode in which shearing occurs with a granular material, powder or fluid layer that separates the blocks (Fig. 1b) (Rabinowicz *et al*. 1961; Godet 1984; Fillot *et al*. 2007).

The wear of fault blocks into gouge powder is an energy dissipative process, and thus its intensity contributes to the frictional resistance of the fault (Byerelee 1967; Power *et al*. 1988; Wilson *et al*. 2005). Moreover, the gouge properties and its evolution apparently control the strength and stability of the fault (Han *et al*. 2010; Reches and Lockner

[1] Geological Survey of Israel, 30 Malkhei Israel St., Jerusalem, Israel. E-mail: vladi@geos.gsi.gov.il

[2] Earth and Planetary Sciences, Washington University, One Brooking Drive, St. Louis, MO 63130, USA.

[3] School of Geology and Geophysics, University of Oklahoma, Norman, OK 73019, USA.

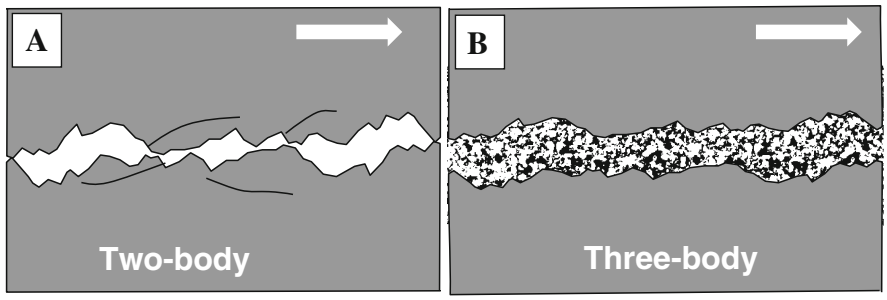

Figure 1
Schematic illustration of a fault zone in two-body (**a**) and three-body modes (**b**). In two-body mode, the sliding blocks interact at touching asperities that reflect the surface roughness. In three-body mode, the sliding blocks are separated by a gouge layer, and wear accumulation occurs at the rock-gouge contact

2010). Whereas wear of bare rock blocks was studied experimentally and theoretically (Wang and Scholz 1994; Power *et al.* 1988; Brodsky *et al.* 2011), fault wear in a third-body setting is yet poorly understood; we propose here a wear model for this configuration.

The present model utilizes the damage rheology approach (Lyakhovsky *et al.* 1997) for the analysis of rock wear. First, we outline the model's approach and describe the friction and wear-rate observations during slip along experimental faults (Boneh *et al.* 2013; Reches and Lockner 2010). Then, we use the key results of the damage rheology model, which are presented in the "Appendix", to evaluate the wear-rate of the present experiments. Finally, we discuss the implications of the present model for natural faults.

2. Wear Rate Model

2.1. Concepts and Assumptions

The common model for wear between sliding solid blocks (Archard 1953; Archard and Hirch 1956) states that the wear volume, WV, follows the relation

$$\mathrm{WV} = K \times D \times \frac{P}{H} \qquad (1)$$

where K is a dimensionless probability constant, D—slip distance, P—applied normal load, and H—hardness of the softer component of the slipping system or flow pressure. The Archard model is based on the assumption that wear occurs at the real contact area between the sliding surfaces, e.g., the touching asperities (Fig. 1a), which is significantly smaller than the nominal area. Queener *et al.* (1965) experimentally recognized an initial transient stage with high wear production, which is termed "running-in". The combined wear model, high running-in wear-rate (Queener *et al.* 1965) followed by lower steady-state wear-rate (Eq. 1) was applied to many experimental analyses of slip between two solid blocks (e.g., Queener *et al.* 1965; Levy and Jee 1988; Kato and Adachi 2000, Wang and Scholz 1994; Boneh *et al.* 2014). However, recent experimental analyses of shearing rock faults demonstrated that Archard's model cannot explain some central observations of fault wear. Hirose *et al.* (2012) found that wear-rates at steady-state conditions strongly depend on slip velocity, which is not considered in Archard's model. They found that granite samples displayed power relations of wear-rate, whereas a negligible wear-rate value was measured for sandstone samples during high velocity runs. Boneh *et al.* (2013) further found that the values of wear-rate and frictional strength in carbonate rocks are interconnected and depend on both slip-velocity and normal stress.

Following these experiments, we present here a new, general model for wear at steady-state slip. The model incorporates the effects of both normal stress and slip velocity, and it shows that Archard's model is a special case of a more general behavior. Our model is based on the following plausible assumptions:

1. Steady-state fault slip occurs in three-body configuration in which a gouge layer separates the rock blocks (Fig. 1b) (Boneh *et al*. 2014).
2. The wear of the rock blocks occurs at the rock-gouge contact (Sagy and Brodsky 2009; Heesakkers *et al*. 2011a, b).
3. The solid rock wears by microfracturing-induced damage, which is controlled by the shear stresses at the rock-gouge contact.
4. Once the microfractures reach a critical density, the solid rock disintegrates and its fragments merge with the gouge zone.

We envision the above process as a microfracturing/damage front that propagates into the solid rock and consider the front velocity as the steady-state wear-rate. Modeling fault wear according to the above assumptions is accomplished here by application of damage mechanics that was developed to quantify brittle rock evolution during continuous deformation (e.g., Krajnovic 1996; Allix and Hild 2002). We show below that (a) wear evolution can be modeled in the framework of phase transition, while the shear kinematics is controlled by the resistance to shear (Lu *et al.* 2007; Lyakhovsky and Ben-Zion 2014a, b); and (b) wear-rate is a function of the system shear and the normal stresses. Finally, we test the validity of the present model by comparing the theoretical predictions with wear-rate observations of experimental faults made of carbonate rock (Boneh *et al.* 2013) and tonalite (Reches and Lockner 2010).

2.2. *Damage Rheology*

Models of damage rheology account for evolving elastic/plastic properties of a deforming body in terms of a "damage-state" variable that most likely represents the local density of micro-cracks. This concept is supported by the observations of gradual accumulation of distributed micro-cracks, their coalescence and localization in a narrow, highly damaged zone with strong micro-crack interaction prior to failure (e.g., Lockner *et al*. 1992; Zang *et al*. 2000; Reches and Lockner 1994). The continuum damage mechanics, which provides a general framework for the rheological behavior during failure processes, has been based on pioneering works by Robinson (1952), Hoff (1953), Kachanov (1958, 1986) and Rabotnov (1959, 1988) and been further developed in engineering (e.g., Hansen and Schreyer 1994; Kachanov 1994; Krajcinovic 1996; Lemaitre 1996; Allix and Hild 2002) and the earth sciences (e.g., Newman and Phoenix 2001; Bercovici *et al*. 2001; Bercovici and Ricard 2003; Shcherbakov and Turcotte 2003; Turcotte *et al*. 2003; Ricard and Bercovici 2009; Karrech *et al.* 2011). The most important advantage of these and other continuum damage mechanics model formulations is that they account for the time-dependent gradual micro-crack accumulation. This is the main difference between damage mechanics and classical fracture mechanics or elasto-plastic models which postulate that failure occurs at given yielding stress conditions ignoring time-dependency of the fracture process. The damage rheology model is capable in reproducing the main stages of the faulting process starting from subcritical crack growth at very early stages of loading, material degradation due to increasing crack concentration, macroscopic brittle failure, post failure deformation, and healing. This physical framework allows modeling the evolution of various fields and properties in laboratory experiments of brittle deformation as well as simultaneous evolution of damage and its localization into narrow highly damaged zones (faults) at crustal scale, earthquakes and associated deformation fields.

Strong micro-crack interaction in a small, intensely damaged volume prior to failure (e.g., Reches and Lockner 1994) raised the need for a non-local model, in which the constitutive relation at a given position is substituted by a law accounting for the spatial distribution of the state variable over a selected neighborhood. The concept of non-local continuum was first introduced to model small-scale effects and heterogeneities in elastic solids (e.g., Eringen 1966; Kroner 1968; Bazant 1991). Non-local models, either integral or gradient type (e.g., Bazant and Jirasek 2002), account for strong micro-crack interaction in a highly damaged area prior to total failure and are capable of reproducing size effect (e.g., Bazant 2005). In this study we use the simplified 1-D version of the model formulated by Lyakhovsky *et al*. (2011) and further developed in Lyakhovsky and Ben-Zion (2014a, b), where

complete thermodynamic derivations are presented. Lyakhovsky and Ben-Zion (2014b) utilized a three-body configuration and simulated frictional response including transitions from high quasi-static friction values at low slip velocity to dynamic friction at high slip rates, but ignored the wear process addressed in the present study.

2.3. Damage Front Propagation

Lyakhovsky *et al.* (2011) recently derived a gradient-type damage formulation that incorporates non-local behavior by enriching the local constitutive relations with a gradient of the damage-state variable. Damage accumulation, $\alpha(x, t)$, in their simplified, 1-D case is

$$\frac{\partial \alpha}{\partial t} = \frac{\partial^2 \alpha}{\partial x^2} + f(\alpha), \tag{2}$$

This equation has the form of the well-known Fisher-KPP reaction–diffusion type equation, or diffusion equation with non-linear source function $f(\alpha)$ (Fisher 1937; Kolmogorov *et al.* 1937) that was extensively applied in a wide range of models in biology, social science, phase transition and critical phenomena (e.g., Grindrod 1996; Murray 2002; Lifshitz and Pitaevskii 1981; Ma 2000). The solution of the Fisher-KPP Eq. (2) exhibits traveling waves or fronts switching between equilibrium states. Travelling fronts propagating with the speed c exist in homogeneous media when $c \geq c_* \equiv 2\sqrt{f'(0)}$, where c_* is a critical speed. The front profile satisfies exponential decay (with algebraic correction) when $c = c_*$ and may fail propagating in heterogeneous media (e.g., Nolen *et al.* 2012). The general form of the source term $f(\alpha)$ in the equation for the damage evolution (2) is discussed by Lyakhovsky and Ben-Zion (2014b) and is given here in the "Appendix" (Eq. 4). The calculated rate of damage accumulation under the conditions that mimic the experimental set-up ("Appendix") leads to the analytical estimation for the speed of the propagating damage front.

2.4. Wear Model Predictions

In the present model, we assume that a narrow, highly damaged band (wear zone) exists between the shearing rock blocks, and thus the shear occurs in a "three-body" mode (Fig. 1b). We model the fault wear as a front that separates between the intensely damaged zone (gouge) and the intact rock. In this 1-D configuration, the wear-rate is the travelling speed, c (measured by volume per unit contact area per time), of the propagating front into the intact rock under steady-state conditions. The present derivations ("Appendix") expresses the wear-rate, WR as a function of the normal stress, σ_n, and friction coefficient, μ_S, during steady-state slip (3a); this relation can also be written as a function of the steady-state shear stress, τ_S (3b):

$$\mathrm{WR} = F \times \sigma_n \sqrt{\mu_S^2 - \mu_{cr}^2} \tag{3a}$$

$$\mathrm{WR} = F \times \sqrt{\tau_S^2 - \tau_{str}^2} \tag{3b}$$

This expression includes two adjustable material parameters, F, and μ_{cr} (or τ_{str}), which is a critical strength parameter of the rock blocks. For constant slip velocity the wear rate represents widening of the damaged band (wear layer) per unit slip distance instead of time. For contact area this is equivalent to wear volume rate per slip distance (Archard 1953). The scaling dimensional parameter F is in some sense equivalent to K in Eq. 1. The rock strength parameter, τ_{str}, is the minimum shear stress necessary for micro-fracturing of the host rock. The values of F and μ_{cr} (or $\tau_{str} = \mu_{cr} \times \sigma_n$) are expected to depend only on the rock type, and to be independent of normal stress and slip velocity, while the confining pressure effect is very weak.

Equations (3a, b) reveal two wear regimes: (1) fault wear when μ_S exceeds a critical, threshold value, $\mu_S \geq \mu_{cr}$ (or applied stress exceeds the material strength, $\tau_S \geq \tau_{str}$), which provides a positive expression under the radical, and (2) no fault wear at lower friction ($\mu_S < \mu_{cr}$) (or lower stress $\tau_S < \tau_{str}$), which implies that the damage front does not propagate at the specified stress conditions. We test the quality of Eqs. (3a, b) by its application to relevant experimental results.

3. Model Application

3.1. Experimental Case Study

We apply our model (Eqs. 3a, b, "Appendix") to the results of Boneh *et al.* (2013) who measured the wear-rates and friction coefficients of experimental

fault made of carbonate rocks. They used a high-velocity, rotary shear apparatus (Reches and Lockner 2010) to shear solid rock samples with ring-shaped contact (5.4 and 7.6 cm inner and outer diameters). Three rock types were used: Kasota dolomite, Dover limestone and a sample containing an upper Kasota dolomite and a lower Blue quartzite. Boneh *et al.* (2013) performed 87 experiments with total slip of 2–28 m at normal stresses between 0.25 and 6.9 MPa. The experiments included 72 constant-velocity experiments and 15 stepping-velocity experiments at a slip velocity range of 0.002–0.96 m/s.

Boneh *et al.* (2013) found that the steady-state friction coefficient μ_S of the tested carbonate faults correlates best with the experimental power-density (shear stress times slip velocity). Figure 2a presents the steady-state friction coefficients, μ_S, measured as a function of normal stress and slip velocity in all tests of the Kasota dolomite and Dover limestone, whereby both upper and bottom sheared surfaces are from the same lithology. Under slow slip velocity (below $\sim$0.01 m/s) the μ_S is high in the range of 0.6–0.8 with a minor decrease under elevated normal stress. The most significant feature of Fig. 2a is the steep decrease of μ_S as the slip velocity increases from $\sim$0.01 to $\sim$0.3 m/s.

Boneh *et al.* (2013) followed Reches and Lockner (2010) and calculated the continuous wear-rate along the experimental faults in terms of wear-rate = [fault-normal shortening]/[slip distance], with units of [micron/m]. Boneh *et al.* (2013) found that the wear-rates during steady-state slip also depend on both slip velocity and normal stress. At low velocity, $V < 0.1$ m/s, the wear-rate linearly depends on the normal stress, whereas at high velocities, $V > 0.3$ m/s, the wear-rate decreases with increasing normal stresses. In these experiments, the wear-rates approach zero at the highest velocities, $V \sim 1$ m/s, and normal stresses, $\sigma_n \sim 7$ MPa.

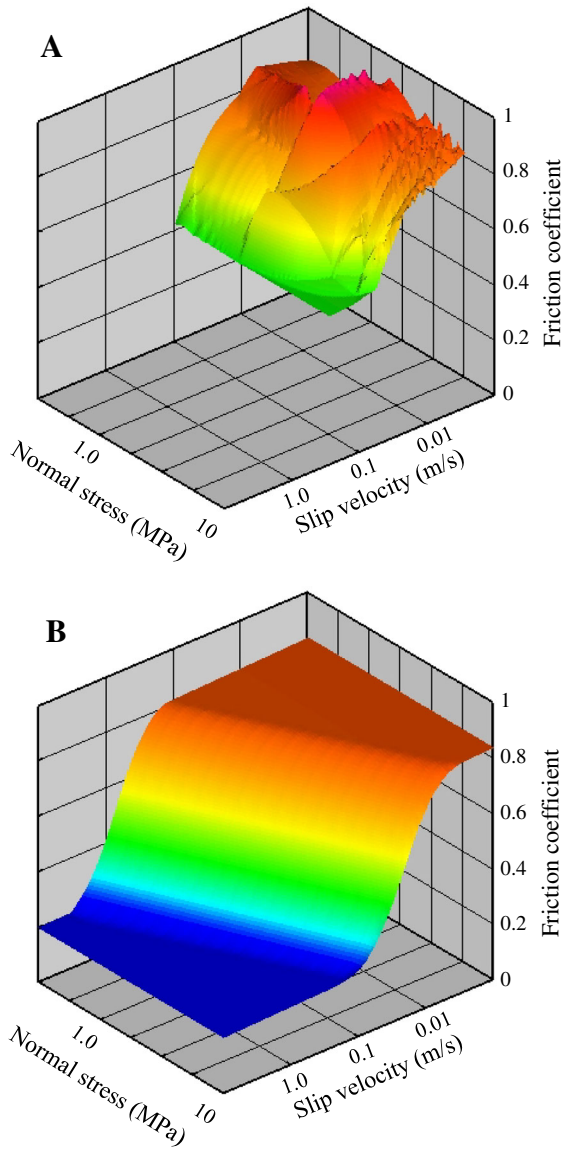

Figure 2
Steady-state friction coefficient as a function of slip velocity and normal stress. **a** Interpolation of 87 results of two sets of dynamic shear experiments (dolomite on dolomite and limestone on limestone), modified after Boneh *et al.* (2013). **b** Generalized function pointing to significant friction decrease in the transition zone and about constant value at higher slip-rate values

3.2. Model Adjustments

To apply the present model to the above experimental results, we first generalized the trend of the experimental frictional results (Fig. 2a) to a simpler trend (Fig. 2b), in which high, constant friction values are set at low velocity and a steep friction drop is set for 0.01–0.1 m/s velocity increase. The friction values are about constant at high slip velocities. A similar steep drop of friction values was observed in laboratory experiments with different rock types (e.g., Di Toro *et al.* 2011). A cross-section of this function (Fig. 3a, black line) displays the relations between slip velocity and steady-state

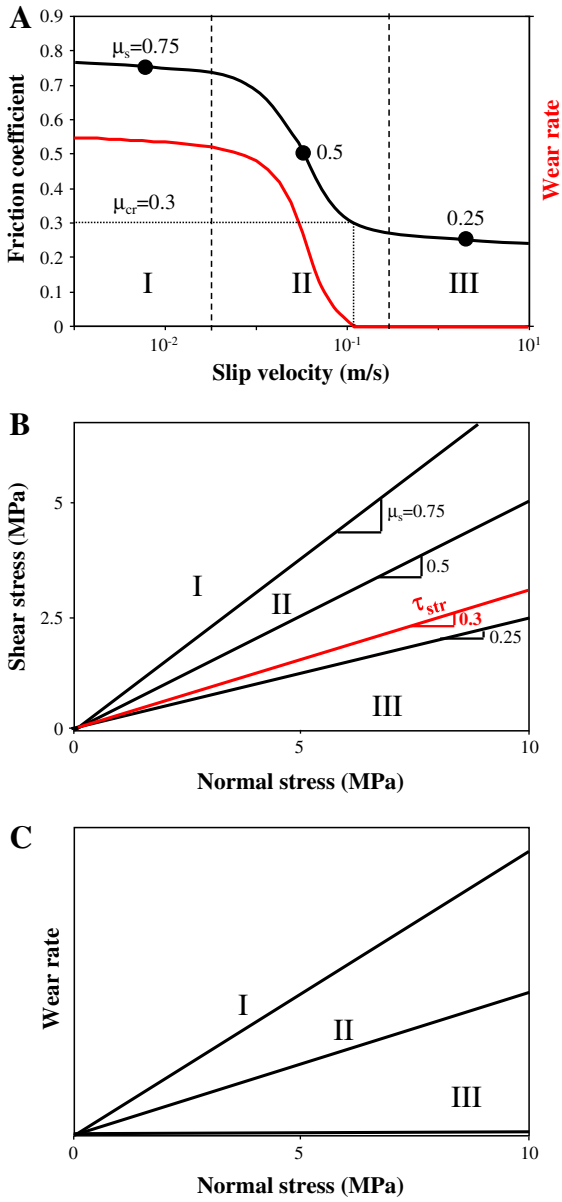

Figure 3
Present model predictions. **a** Schematic relationship between steady-state friction and slip velocity at constant normal stress (*black line*). *Red line* shows calculated wear-rate. Three regimes of steady-state frictional strength are marked: (*I*)—high friction at low slip velocity; (*II*)—steep drop with increasing slip rate; (*III*)—low friction at high slip-rates. Wear-rate drops to zero at critical friction coefficient μ_{cr}. **b** Shear versus normal stress for frictional values representing three different regimes. *Red line* shows shear stress corresponding to material strength for $\mu_{cr} = 0.3$. **c** Wear-rate versus normal stress for the same regimes

friction at constant normal stress. Three model regimes of steady-state frictional strength are built into Figs. 2b and 3a:

Regime I—high, quasi-constant μ_S of 0.7–0.8 at low slip velocity;
Regime II—steep drop rate of μ_S with increasing slip-rate;
Regime III—low, quasi-constant μ_S at high slip-rates.

Our model predicts that the wear-rate is proportional to the shear stress (Eq. 3b); this dependence is a natural outcome of model assumption #3 above. Thus, under constant normal stress, the wear-rate (red curve in Fig. 3a) dependence on slip velocity is predicted to mimic the dependence of friction coefficient μ_S (black curve in Fig. 3a). In this respect, similarly to the FILLOT *et al.* (2007) model, our model links the fault wear to the shear resistance of the fault during steady state. The model predicts significantly different wear-rates associated with three frictional regimes: high wear-rates in regime I, transitional wear-rates in regime II and vanishing wear-rates in regime III. Furthermore, the wear-rate drops when $\mu_S \rightarrow \mu_{cr}$ (Eqs. 3a, b) and may even vanish when the frictional strength decreases below the defined critical value ($\mu_S < \mu_{cr}$) (Fig. 3a). These wear-rate variations may be expressed in terms of the applied stress (Fig. 3b). The red line in Fig. 3b shows the material strength versus normal stress for the selected $\mu_{cr} = 0.3$. Under loading conditions corresponding to $\mu_S = 0.75$ or 0.5 the shear stress is above the material strength (lines I and II in Fig. 3b). These stress conditions favor micro-fracturing in the form of a propagating damage front into the solid rock. In the case of low shear stresses in regime III with $\mu_S = 0.25$, the shear stress is below the material strength, which is the threshold for micro-crack nucleation and growth; with no rock damage, fault slip might continue without wear.

Figure 3c displays the expected relations between normal stress and wear-rate for the three regimes of Fig. 3a. The wear-rate is expected to linearly increase with respect to the normal stress, as in Archard's

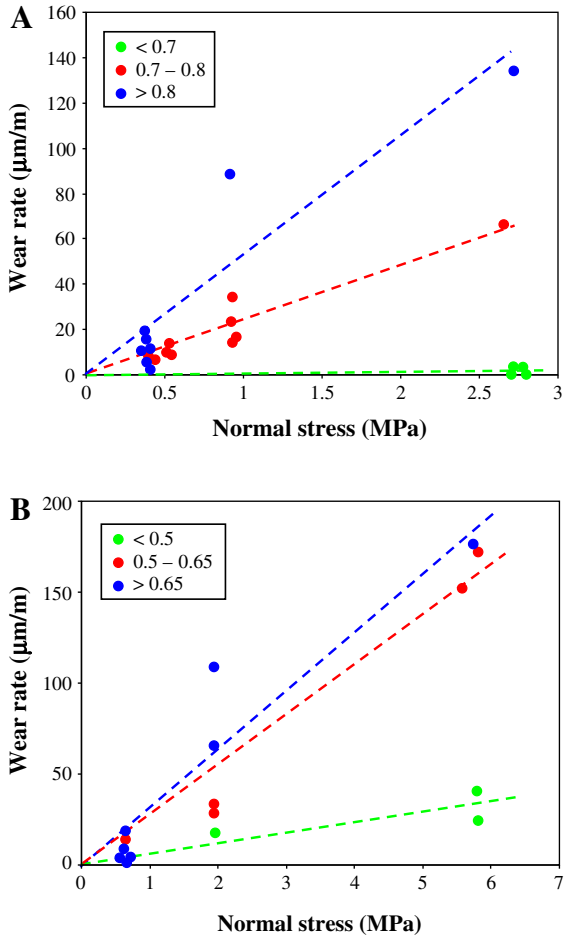

Figure 4
Experimentally measured wear-rates under steady-state conditions (after Boneh *et al.* 2013) for Dover limestone faults (**a**), and for samples composed of an upper Kasota dolomite and a lower Blue quartzite (**b**). *Colored points* are grouped according to the range of the measured friction coefficient (*inset*). *Dashed lines* with the same color are the model-predicted wear-rates according to the frictional value for each group

model, but at a different slope that depends on the steady-state friction. The slopes marked I–III in Fig. 3c correspond to the representative friction values of $\mu_S = 0.75$ and 0.5 for the regimes I and II and is zero (no wear) for $\mu_S = 0.25$ in regime III.

3.3. *Comparison of Experimental Results and Model Predictions*

3.3.1 *Carbonate Faults*

The experimentally measured wear-rates are now compared with the predicted trends of the model.

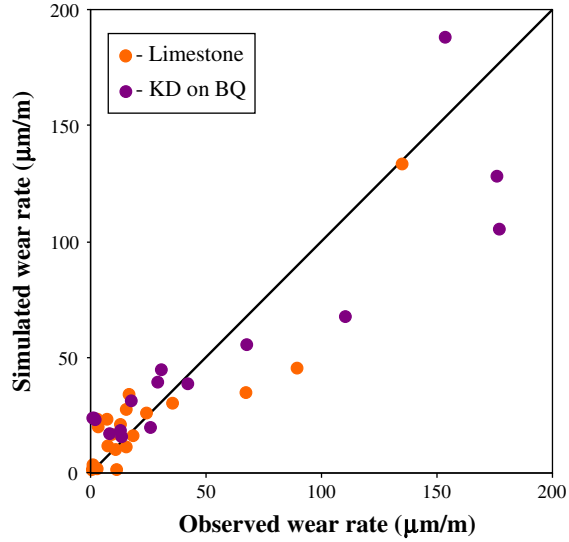

Figure 5
Model simulated versus experimentally observed wear-rates for the two sets of experiments shown in Fig. 4

Figure 4 shows measured wear-rates reported by Boneh *et al.* (2013) for Dover limestone samples (Fig. 4a) and for samples containing an upper Kasota dolomite and a lower Blue quartzite (Fig. 4b). Experimentally measured wear-rates were fitted with the model Eq. (3a) using least-squares by changing two parameters, material constant F and critical friction coefficient μ_{cr}. The best fitting model parameters are: $F = 98.4$ µm m^{-1} MPa^{-1}, $\mu_{cr} = 0.68$ for Dover limestone, $F = 49.8$ µm m^{-1} MPa^{-1}, $\mu_{cr} = 0.35$ for Kasota dolomite on Blue quartzite. Experimental results for each rock type are plotted in three groups according to the observed steady-state friction value. The modeled trend lines (dashed lines with the same color as markers representing specific group) are the calculated linear relations between the experimental wear-rate and normal stress for the given friction group. The systematic slope decrease with decreasing friction coefficients fits the model predictions. Comparison of the experimentally observed wear-rates with the model's calculated wear-rates (Eq. 3a) in Fig. 5 indicates that the simplified 1-D model reproduces the general trends of the wear-rate changes with both normal stress and frictional strength.

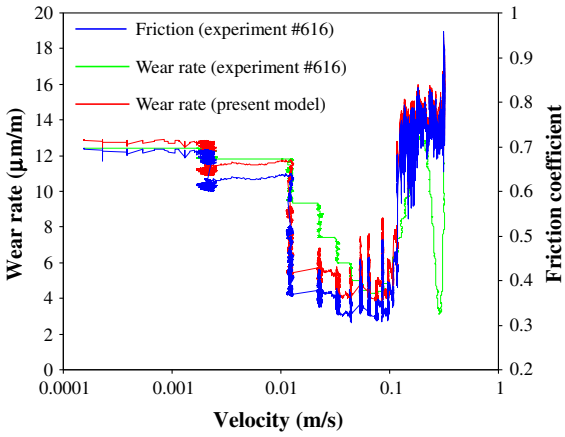

Figure 6
Wear-rate and friction coefficient during rotary shear experiment (#616 in Reches and Lockner 2010) plotted with wear-rate predictions of the present model. The experiment was conducted on a tonalite (Sierra White granite) sample at normal stress of 3.05 MPa with total slip of 65 m at 30 slip velocity steps (see text)

3.3.2 Tonalite Fault

An extensive series of friction experiments on samples of tonalite, which is better known by its commercial name Sierra White granite (SWG), were reported by Reches and Lockner (2010). We apply the present model to their experiment #616 that was conducted at a constant normal load of 3.08 Mpa and stepping velocity. This experiment was conducted on the same rotary apparatus and similar sample geometry as Boneh *et al.* (2013), but differs in two central parameters: rock composition and loading configuration. The #616 experimental fault was made of tonalite, an igneous rock dominated by quartz and feldspar (Reches and Lockner 2010), whereas Boneh *et al.*'s (2013) experiments were conducted on limestone and dolomite samples. Also, experiment #616 was subjected to a continuous sequence of 30 slip velocity steps from $V = 0.0015$ to 0.32 m/s, and the slip distance during each velocity step was 2.1 m; on the other hand, the reported experiments in Fig. 4 are single velocity runs. The experimental results of #616 (Fig. 6) are shown by friction coefficient (blue line) and wear-rate (green line) as a function of the changing slip velocity. We used Eq. (3a) to calculate the expected wear-rates for the measured friction coefficient, and the red line in Fig. 6 is the calculated curve for $F = 6.5\ \mu m\ m^{-1}\ MPa^{-1}$, $\mu_{cr} = 0.25$. Instead of the best-fit procedure, these values were chosen to reproduce high wear-rate values during the initial experimental stages with low slip velocities (up to 0.01 m/s), and the low wear-rate values for the velocity range between 0.01 and 0.1 m/s. The present model based on steady-state conditions is not expected to fit experimental results of transient conditions which are intrinsic for stepping velocity experiments. Therefore, the least-squares procedure was not applied to the measured data.

In spite of the transient nature of #616 experiment, the present model, provides a reasonable fit to the experimental data, and predicts the main features of the observations: (1) abrupt wear-rate decreases as the friction coefficient drops from $\sim$0.7 to $\sim$0.4 (slip velocity $\sim$0.01 m/s). Yet, the measured wear-rate decreases gradually, whereas the model's calculated wear-rate drops abruptly. This difference is probably associated with transient change of the wear-rate that under changing velocities does not reach the steady-state of the presented model. (2) At higher velocities (above 0.1 m/s), the experimental friction coefficient abruptly increases (due to temperature rise, Reches and Lockner 2010; Sammis *et al.* 2011), as well as the experimental and model-derived wear-rates. Note again a delay of the rise of the experimental wear-rate. We also note that the model fails to predict the abrupt drop of wear-rate at the high-velocity of V 0.22–0.29 m/s). Nevertheless, the successful model simulation of the wear-rates in experiment #616 further indicate the strong correlation between frictional strength and wear-rate even under transient slip conditions.

4. Discussion

4.1. Relations to Archard's Wear Model

We derived the model for wear-rate of rock faults under steady-state conditions with constant slip velocity and loading stresses motivated mainly by the limited ability of the well-known Archard (1953) model to explain recent experimental observations of rock wear (Hirose *et al.* 2012; Boneh *et al.* 2013). Archard's (1953) model was based on wear at

contacting asperities (Fig. 1a), implying that the wear-rate is proportional to a strength ratio of [normal stress]/[hardness of the softer surface] (Eq. 1). The mechanical conditions at the contacting asperities (e.g., gouge presence, roughness, and lubrication) were integrated into one free parameter, K. In contrast, our model is derived for slip in a three-body mode (Fig. 1b) with a gouge layer separating the blocks; experimental (Reches and Lockner 2010; Boneh *et al.* 2014) and field observations (e.g., Chester and Chester 1998; Katz *et al.* 2003) indicate that this is the realistic mode for steady-state slip. In the model, the wear process is associated with microfracturing and gradual damage increase in the solid rock.

We analyze the wear process by using a non-local continuum damage mechanics connecting wear-rate with the rate of a propagating damage front. The evolving material damage in space and time is defined by the reaction–diffusion equation with non-linear source term (Eqs. 7, 8) known as Fisher-KPP equations. Using the general properties of the mathematical solution of Fisher-KPP equations, we can quantify the process dynamics without calculating local state and motion of every single crack in the system. The derivations lead to a simple expression, Eqs. (3a, b), connecting the wear-rate with the frictional strength of a fault. Comparison with experimental data demonstrates that our wear model is capable of predicting the wear-rates under a wide range of slip velocities and normal stresses (Figs. 4, 6) (Eqs. 3a, b). The model depends on the critical strength of the host rock, τ_{srt}, or its equivalent, the critical friction coefficient, μ_{crt}. Archard's model appears as a specific case in which the friction coefficient is constant and larger than the critical friction coefficient, μ_{crt}, (as the wear-rate vanishes when $\mu \leq \mu_{crt}$). Moreover, we showed in the "Appendix" that the model is valid and even simpler for wear in relatively large confining pressures and significant degradation of the shear modulus (Fig. 7), which are the conditions assumed for natural faulting, but until now, have never been taken into account in wear models. Considering these intrinsic limitations of Archard's model, its application to field cases of natural faulting is limited, as shown below.

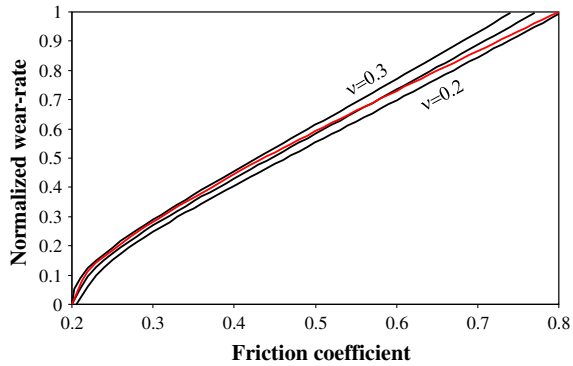

Figure 7
Normalized wear-rate versus friction coefficient calculated using (14) with Poisson ratio, $\nu = 0.2$, 0.25 and 0.3 (*black lines*). *Red line* shows suggested approximation (15) used in this study

4.2. Wear, Gouge Thickness and Fault Slip Distance

The present analysis provides an important insight on gouge accumulation along faults. It is assumed here that at steady-state, the front of fault wear propagates into the host rock by micro-cracking damage. Based on this assumption, the wear-rate has simple relations to the friction coefficient ("Appendix", Fig. 3, Eq. 3a) or shear-stress (Eq. 3b). Now, when the shear-stress drops, e.g., due to a friction coefficient drop at high slip velocity, the wear-rate also drops (Fig. 6), or even vanishes when $\mu_S < \mu_{cr}$ (Figs. 3, 4, Eqs. 3a, b). An obvious deduction from these results is that a fault may slip over long distances without ongoing wear and thickening of the gouge zone if the shear stress (or the equivalent friction coefficient) is low enough. This conclusion leads to a new view on gouge-zone thickness (discussed below).

As fault gouge is the main wear product of fault slip, it is commonly envisioned that gouge continuously forms and accumulates during fault slip (e.g., Scholz 1987). It was thus suggested that the total gouge thickness, G_T, along a given fault is proportional to the total slip distance, D, of the fault. Scholz (1987) showed that this relation is a natural result of Archard's model, and used compiled field data to demonstrate that G_T is linearly proportional to the total fault slip with $G_T/D = 0.1$–0.001 over about seven orders of magnitude of fault slip. Interestingly, based on fractal fault geometry and transient wear mechanism, Power *et al.* (1988) also suggested that

wear zone thickness of natural faults depends linearly on displacement, because the size of the asperities increases in an approximately linear relationship to displacement. On the other hand, based on fault surface roughness measurements and contact mechanics, Brodsky *et al.* (2011) predicted that average wear-rate is a weak function of D (proportional to D^{-1}); therefore, even under infinite fractal roughness the wear-rate is not constant. According to Brodsky *et al.* (2011), the predicted wear-rate vanishes, or $G_T \sim$ constant, for faults that already accumulated large slip distances. These works were based on an asperity failure concept (Fig. 1a), and considered the effects of roughness, lithology and normal stresses on wear-rate (Scholz 1987; Wang and Scholz 1994; Power *et al.* 1988; Brodsky *et al.* 2011), but implicitly ignored the intensity of the fault-parallel shear-stress. On the other hand, our model considered the three-body configuration (Fig. 1b) in which the wear-rate depends on the shear-stress intensity at the gouge-rock contact (Eqs. 3a, b).

Our model results can now be applied to evaluate fault wear at seismic conditions. Experimental works have shown that the dynamic friction during high slip velocity may be as low as 0.1–0.3, as shown in many high-velocity friction experiments (Reches and Lockner 2010; Di Toro *et al.* 2011; Chang *et al.* 2012) or even vanish at seismic velocities (Han *et al.* 2010). Application of these experimental observations to the field indicates that earthquake slip could generate very low wear, and thus the long-term gouge accumulation along a seismically active fault is not necessarily related to its total slip (Shipton *et al.* 2006). For example, Chester *et al.* (1993) analyzed two major branches of the San Andreas system, the north branch San Gabriel and Punchbowl faults, with a total slip of 22 and 44 km, respectively. They showed that almost the entire slip along these faults was localized within a 1 m thick zone of cataclasite (=cohesive gouge). According to Scholz's (1987) compilation of $G_T/D = 0.1$–0.001, the minimum expected gouge thickness of these faults is on the order of tens of meters. Thus, our model, which predicts negligible wear for faults with low to vanishing dynamic friction, provides a suitable interpretation for the observed gouge thickness along active faults such as the north branch San Gabriel and Punchbowl, California.

Our model predictions may also hold for faults that are intrinsically weak due to their composition. For example, Lockner *et al.* (2011) analyzed the strength of core materials collected from the San Andreas fault-zone, California. The core was retrieved from a depth of 2.7 km in the creeping segment of the host fault. The strength measurements conducted at in situ conditions revealed a very weak gouge, with a friction coefficient of ~ 0.15, due to the presence of saponite, which is an extremely weak phyllosilicate mineral. According to our model, faults with such low static frictional strength will undergo negligible wear and consequently will have anomalously thin gouge zones.

The present model is a simplified one that fits well the simple configuration of the experimental faults. However, the wear of natural faults can also be affected by additional parameters such as pre-faulting damage, variable slip velocity, complex geometrical, lithological and rheological relations (e.g., Katz *et al.* 2003; Brodsky *et al.* 2011; Nielsen *et al.* 2010).

5. Summary and Conclusions

The present wear model is based on a continuum damage-breakage rheological model that provides a general quantitative description of fault mechanics (Lyakhovsky and Ben-Zion 2014b). This model considers a transition from a solid phase with distributed fracturing and evolving elastic moduli to a granular phase referred to as pseudo-liquid. The model of Lyakhovsky and Ben-Zion (2014b) reproduces central features of a fault-zone structure, including slip localization within a narrow zone, gouge formation (three-body mode), and transition between slow motion associated with high steady-state friction to a dynamic regime with low friction. The present wear model is a 1-D simplification of the general formulation ("Appendix") that leads to a general expression for wear-rate under steady-state slip (Eqs. 3a, b).

The present analysis leads to the following conclusions:

1. The theoretical wear-rate of a fault during steady-state slip (Eqs. 3a, b) is linked to the shear stress along the slipping fault: It is relatively high when

the shear stress, τ_s, is much higher than the rock strength, τ_{str}, it drops as the shear stress drops, and the wear-rate vanishes when the shear stress is lower than the rock strength.

2. The model successfully predicted the wear-rate intensities in two sets of friction experiments (Boneh *et al.* 2013; Reches and Lockner 2010). These experiments were conducted on different rocks (limestone, dolomite and tonalite), a wide range of slip velocities (0.001–0.97 m/s), and two types of loading histories (constant slip velocity or stepping velocity).
3. This successful application to experimental observations indicates that the central model concept of damage-driven wear in a "three-body" configuration (Fig. 1b) is a reasonable approach for wear under steady-state slip. We conclude that this concept is more realistic than the asperities contact model of bare rock surfaces (Fig. 2a).
4. The present wear model suggests that the thickness of gouge (cataclasite) layers along a natural fault strongly depends on their frictional strength, and thus faults with low frictional resistance (static and/or dynamic) may slip with low to negligible wear.

Acknowledgments

The manuscript benefitted from useful comments by Y. Ben-Zion (editor), W. Ashley Griffith (reviewer), and an anonymous reviewer. The study was supported by the NSF, Geosciences, Equipment and Facilities, Grant No. 0732715, with partial support of NSF, Geosciences, Geophysics, Grant No. 1045414, and ConocoPhillips Foundation grant. VL acknowledges support by the US–Israel Binational Science Foundation (Grant 2008248); AS acknowledges support by the Israel Science Foundation (Grant 929/10).

Appendix

Damage Rheology Model

Key derivations of the damage rheology model leading to the estimate of the speed of the propagating damage front are presented in this "Appendix". Following thermodynamic balance relations and the Onsager (1931) principle, Lyakhovsky *et al.* (1997) developed a kinetic equation for the damage state variable, α (weakening and healing) which is a function of the progressive deformation. Non-linear elasticity that connects the effective elastic moduli to a damage variable and loading conditions allows accounting for the transition from damage accumulation to healing. This transition is controlled by the strain invariants ratio $\xi = I_1/\sqrt{I_2}$, where $I_1 = \varepsilon_{kk}$ and $I_2 = \varepsilon_{ij}\varepsilon_{ij}$ are the invariants of the elastic strain tensor ε_{ij}. The ξ value is a conjugate quantity to the ratio between shear and normal stress expressed in terms of strains, instead of stresses. The rate of damage/healing accumulation is given by Lyakhovsky *et al.* (1997):

$$\frac{d\alpha}{dt} = \begin{cases} C_d I_2(\xi - \xi_0) & \text{for } \xi > \xi_0 \\ C_1 \exp\left(\frac{\alpha}{C_2}\right) I_2(\xi - \xi_0) & \text{for } \xi < \xi_0 \end{cases} . \quad (4)$$

where the coefficient C_d is the rate of positive damage evolution (material degradation) that is constrained by laboratory experiments (Lyakhovsky *et al.* 1997; Hamiel *et al.* 2004, 2006). The value $\xi = \xi_0$ controls the onset of damage accumulation or transition from material healing to weakening associated with microcrack nucleation and growth. The value of the critical strain invariants ratio also called "modified internal friction" (see Fig. 3 in Lyakhovsky *et al.* 1997) is explicitly related to the internal friction angle of Byerlee's law (Byerlee 1978) and Poisson ratio of the intact rock.

The rate of damage recovery (healing) is assumed to depend exponentially on α and produces logarithmic healing with time in agreement with the behavior observed in laboratory experiments with rocks and other materials (e.g., Dieterich and Kilgore 1996; Scholz 2002; Muhuri *et al.* 2003; Johnson and Jia 2005). Lyakhovsky *et al.* (2005) showed that the local damage model reproduces the main phenomenological features of the rate- and state-dependent friction, and constrained the healing parameters C_1, C_2 by comparing the model calculations with empiric parameters of the slow-rate frictional sliding (e.g., Dieterich 1972, 1979; Marone 1998).

The damage accumulation under constant stress in a simplified 1-D model with effective elastic moduli

degrading proportionally to $(1-\alpha)$ follows a power law solution (e.g., Ben-Zion and Lyakhovsky 2002; Turcotte *et al.* 2003):

$$\alpha(t) = 1 - \left(1 - 3\frac{C_d\sigma^2}{G_0^2}t\right)^{1/3}. \quad (5)$$

where G_0 is the elastic moduli of the intact rock, σ, the applied stress, and C_d the damage rate coefficient. This solution allows us to introduce a time scale, t_f, which is the time-to-failure when $\alpha = 1$ (total damage) (e.g., Paterson and Wong 2005) that becomes

$$t_f = \frac{G_0^2}{3C_d\sigma^2}. \quad (6)$$

This parameter controls the time scale of all processes associated with accumulated damage, including the growth rate of narrow fracture zones.

Recently, Lyakhovsky *et al.* (2011) developed a gradient-type damage rheology formulation that incorporates non-local behavior by enriching the local constitutive relations with a gradient of the damage state variable. This addition modifies the kinetic equation for the damage evolution. In addition to the source term controlling the damage growth in Eq. (4), the damage accumulation for $\xi > \xi_0$ in non-local formulation includes damage diffusion term with a coefficient D:

$$\frac{\partial\alpha}{\partial t} = C_d I_2(\xi - \xi_0) + D\nabla^2\alpha. \quad (7)$$

The non-local gradient-type damage kinetic Eq. (7) has the form of a Fisher-KPP reaction–diffusion type equation for which the general one-dimensional form is

$$\frac{\partial u}{\partial t} = \frac{\partial^2 u}{\partial x^2} + f(u) \quad (8)$$

The solution of the Fisher-KPP Eq. (8) exhibits a traveling wave or fronts switching between equilibrium states $f(u) = 0$ (see text). Travelling fronts propagating with the speed c exist in homogeneous media when $c \geq c_* \equiv 2\sqrt{f'(0)}$. We calculate the source term $f(\alpha) = C_d I_2(\xi - \xi_0)$ for $\alpha = 0$ under loading condition that mimics the experimental set-up with the normal stress σ_n and shear stress τ, and then estimate the speed of the propagating damage front.

Adopting damage model with $(1-\alpha)$ reduction of the elastic moduli, the relations between stress and strain components (axial, ε_a, and transversal, ε_τ) are (E_0, G_0, Young and shear moduli of the intact rock):

$$\varepsilon_a = \frac{\sigma_n}{E_0(1-\alpha)};\ \varepsilon_\tau = \frac{\tau}{2G_0(1-\alpha)} \quad (9)$$

Using relations (9), the second strain invariant, I_2, and strain invariant ratio, ξ, are,

$$I_2 = \varepsilon_a^2 + 2\varepsilon_\tau^2 = \frac{1}{(1-\alpha)^2}\left[\frac{1}{E_0^2}\sigma_n^2 + \frac{1}{2G_0^2}\tau^2\right] \quad (10)$$

$$\xi = \frac{\varepsilon_a}{\sqrt{\varepsilon_a^2 + 2\varepsilon_\tau^2}} = \frac{-1}{\sqrt{1 + 2\left(\frac{E_0\tau}{2G_0\sigma_n}\right)^2}} \quad (11)$$

The minus sign in (11) implies that the compaction strains are negative. Note that without any shear loading ($\tau = 0$), the strain invariants ratio is $\xi = -1$, which is slightly below typical ξ_0 range (Lyakhovsky *et al.* 1997). This implies that damage is not accumulated at loading by normal stress alone without shear loading. Substituting (10, 11) into equation for the damage accumulation (7), leads to the following relation for the source term:

$$f(\alpha) = C_d\frac{1}{(1-\alpha)^2}\left[\frac{1}{E_0^2}\sigma_n^2 + \frac{1}{2G_0^2}\tau^2\right] \times \left[\frac{-1}{\sqrt{1 + 2\left(\frac{E_0\tau}{2G_0\sigma_n}\right)^2}} - \xi_0\right] \quad (12)$$

The speed of the travelling damage front, which in the present work is defined as the wear-rate (text), is controlled by the value $c_* = 2\sqrt{D\cdot f'(0)}$ equal to

$$c_* = 2\sqrt{2C_d D}\frac{\sigma_n}{E_0} \times \sqrt{-\xi_0\left[1 + 2\left(\frac{E_0\tau}{2G_0\sigma_n}\right)^2\right] - \sqrt{1 + 2\left(\frac{E_0\tau}{2G_0\sigma_n}\right)^2}} \quad (13)$$

Taking $\mu_S = \tau/\sigma_n$ for the steady-state friction coefficient, Eq. (13) is rearranged to:

$$c_* = 2\sqrt{2C_d D}\frac{\sigma_n}{E_0}\sqrt{-\xi_0\left(1+A\mu_S^2\right)-\sqrt{1+A\mu_S^2}} \tag{14}$$

where $A = 2(E_0/2G_0)^2 = 2(1+\nu)^2$, and ν is the Poisson ratio. Note that typical values of the strain invariant ratio, ξ_0, controlling the onset of damage accumulation in (4) vary between $\xi_0 = -1.2$ and $\xi_0 = -0.6$. These values are taken from Fig. 3 of Lyakhovsky *et al.* (1997) for friction angle 30°, $\nu = 0.2$ and for friction angle 40°, $\nu = 0.3$. The steady-state friction coefficient should be above certain critical or threshold values ($\mu_S \geq \mu_{cr}$) related to the material strength to give positive expression under the radical in (14). A negative value for $\mu_S < \mu_{cr}$ implies that the applied shear stress is below the level needed for the onset of damage accumulation and the source term in damage growth Eq. (7) is negative; no any damage is accumulated, and no wear is anticipated.

The Poisson ratio for most rocks varies within the small range $\nu = 0.2$–0.3. Variation of the steady-state friction, μ_S, is also limited. It decreases from static friction values about 0.6–0.8 to dynamic values about 0.2–0.4. Accounting for this limited range of the material properties, the speed of the travelling damage front or wear-rate calculated using (14) only slightly depends on the Poisson ratio (black lines in Fig. 7). Hence, the wear-rate may be approximated by much simpler equation (red line in Fig. 7):

$$\text{wear\_rate} \propto \sigma_n\sqrt{\mu_S^2 - \mu_{cr}^2} \tag{15}$$

The units of the speed of the travelling damage front (13, 14) are length per time, while in the laboratory experiments wear-rate measured the thinning of the sample per unit slip. As the area of the surface is constant (Boneh *et al*. 2013), this thinning is proportional to the wear volume generation. Such unit conversion could be done under steady-state conditions with constant slip rate.

We note here that Eq. (14) was derived for the loading conditions of experimental set-up. More appropriate conditions for deep seismogenic zones should account for relatively large confining pressure, small damage-induced change of the bulk modulus and significant degradation of the shear modulus. Similar derivations lead directly to the more simple form (15) instead of (14) for the natural conditions.

References

Allix, O. and Hild, F. (2002) Continuum damage mechanics of materials and structures, Elsevier, 396 pp.

Archard, J.F. (1953) *Contact and rubbing of flat surfaces*, J. Appl. Phys., *24*, 981–988.

Archard, J.F., Hirch, W. (1956) *Wear of metals under unlubricated conditions*. Proc. R. Soc. Lond. A Math. Phys. Sci. *236*, 397–410.

Bazant, Z.P. (1991) *Why continuum damage is nonlocal: Micromechanics arguments*, J. Eng. Mech., 1070–1087.

Bazant, Z.P. (2005) Scaling of structural strength. Elsevier, 327 pp.

Bazant, Z.P. and Jirasek, M. (2002) *Nonlocal integral formulations of plasticity and damage: Survey of progress*, J. Eng. Mech., *128*, 1119–1149.

Ben-Zion, Y., Lyakhovsky, V., (2002), *Accelerating seismic release and related aspects of seismicity patterns on earthquake faults*. Pure Appl. Geophys. *159*, 2385–2412.

Bercovici, D. and Ricard, Y. (2003) *Energetics of a two-phase model of lithospheric damage, shear localization and plate boundary formation*, Geophys. J. Int., *152*, 581–596.

Bercovici, D., Ricard, Y., and Schubert, G. (2001) *A two-phase model for compaction and damage, part 1: general theory*, J. Geophys. Res., *106*, 8887–8906.

Boneh, Y, Chang, J.J., Lockner, D.A., and Reches, Z. (2014) *Fault evolution by transient processes of wear and friction*, Pure. Appl. Geoph. (this volume).

Boneh, Y. (2012) Wear and gouge along faults: Experimental and mechanical analysis, Thesis, Univ. Oklahoma.

Boneh, Y., Sagy, A., and Reches, Z. (2013) *Frictional strength and wear-rate of carbonate faults during high-velocity, steady-state sliding*, Earth Planet. Sci. Lett., *381*, 127–137.

Brodsky E.E., Gilchrist, J.J Sagy, A., and Collettini, C. (2011) *Faults smooth gradually as a function of slip*, Earth Planet. Sci. Lett., *302*, 185–193.

Byerelee, J.D. (1967) *Frictional characteristics of granite under high confining pressure*, J. Geophys. Res., *72*, 3639-3648.

Byerlee, J.D., (1978), *Friction of rocks*. Pure Appl. Geophys., *116*, 615–626.

Chang, J.C., Lockner, D.A., Reches, Z. (2012) *Rapid acceleration leads to rapid weakening in earthquake-like laboratory experiments*, Science, *338*, 101, doi:10.1126/science.1221195.

Chester, F.M., and Chester, J.S. (1998) *Ultracataclasite structure and friction processes of the San Andreas fault*, Tectonophysics, *295*, 199–221.

Chester, F.M., Evans, J.P., Biegel, R.L. (1993) *Internal structure and weakening mechanisms of the San Andreas fault*, J. Geophys. Res., *98*, 771–786.

Chester, F.M., Logan, J.M. (1987) *Composite planar fabric of gouge from the Punchbowl fault, California*, J. Struct. Geol., *9*, 621–634.

Di Toro, G., Han, R., Hirose, T., De Paola, N., Nielsen, S., Mizoguchi, K., Ferri, F., Cocco, M., Shimamoto, T. (2011) *Fault lubrication during earthquakes*. Nature, *471*, 494–498.

Dieterich, J.H. and Kilgore, B.D., (1996), *Imaging surface contacts; power law contact distributions and contact stresses in quarts, calcite, glass, and acrylic plastic*, Tectonophysics, *256*, 219–239.

Dieterich, J.H., (1972) *Time-dependent friction in rocks*. J. Geophys. Res., *77*, 3690–3697.

Dieterich, J.H., (1979) *Modeling of rock friction 1. Experimental results and constitutive equations*, J. Geophys. Res., *84*, 2161–2168.

Engelder, J. T. (1974), *Cataclasis and the generation of fault gouge*. Geol. Soc. Am. Bull., *85*, 1515–1522.

Eringen, A.C. (1966) *A unified theory of thermomechanical materials*, Int. J. Energ. Sci., *4*, 179–202.

Fillot, N., Iordanoff, I., and Berthier, Y. (2007) *Wear modeling and the third body concept*, Wear, *262*, 949–957.

Fisher, R. (1937), *The wave of advance of advantageous genes*, Ann. Eugenics, *7*, 355–369.

Godet, M. (1984) *The third-body approach: A mechanical view of wear*. Wear, *100*, 437–452.

Grindrod, P. (1996) The theory and applications of reaction-diffusion equations: Patterns and waves, Oxford Applied Mathematics and Computing Science Series, The Clarendon Press, Oxford Univ. Press, New York, 2nd ed., 275 p.

Hamiel, Y., Liu, Y., Lyakhovsky, V., Ben-Zion. Y. and Lockner, D., (2004), *A visco-elastic damage model with applications to stable and unstable fracturing*. J. Geophys. Int. *159*, 1155–1165.

Hamiel, Y., Katz, O., Lyakhovsky, V. Reches, R. and Fialko, Y. (2006) *Stable and unstable damage evolution in rocks with implications to fracturing of granite*. Geophys. J. Int. *167*, 1005–1016, doi:10.1111/j.1365-246X.2006.03126.x.

Han, R., Hirose, T., Shimamoto, T. (2010) *Strong velocity weakening and powder lubrication of simulated carbonate faults at seismic slip rates*. J. Geophys. Res., *115*, B03412, doi:10.1029/2008JB006136.

Hansen, N.R. and Schreyer, H.L. (1994) *A thermodynamically consistent framework for theories of elasticity coupled with damage*, Int. J. Solids Struct., *31*, 359–389.

Heesakkers, V., Murphy, S., and Reches, Z. (2011a) *Earthquake rupture at focal depth, Part I: Structure and rupture of the Pretorius fault, TauTona mine, South Africa*, Pure Appl. Geophys., doi:10.1007/s00024-011-0354-7.

Heesakkers V., Murphy. S., Locker, D.A., and Reches, Z. (2011b) *Earthquake rupture at focal depth, Part II: Mechanics of the 2004 M2.2 earthquake along the Pretorius fault, TauTona mine, South Africa*, Pure Appl. Geophys., doi:10.1007/s00024-011-0355-6.

Hirose, T., Mizoguchi, K., Shimamoto, T. (2012) *Wear processes in rocks at slow to high slip rates*. J. Struc. Geol., doi:10.1016/j.jsg.2011.12.007.

Hoff, N.J. (1953) *The necking and rupture of rods subjected to constant tensile loads*, J. Apl. Mech., *20*, 105–108.

Johnson, P.A. and Jia, X., (2005), *Non-linear dynamics, granular media and dynamic earthquake triggering*, Nature, *437*, 871–874.

Kachanov, L.M. (1958) *On the time to rupture under creep conditions*, Izv. Acad. Nauk SSSR, *OTN 8*, 26-31 (in Russian).

Kachanov, L.M. (1986), Introduction to Continuum Damage Mechanics, Martinus Nijhoff Publishers, 135 p.

Kachanov, M. (1994) *On the concept of damage in creep and in the brittle-elastic range*, Int. J. Damage Mech., *3*, 329–337.

Karrech, A. Regenauer-Lieb, K., and Poulet, T. (2011) *Continuum damage mechanics for the lithosphere*. J. Geophys. Res., *116*, B04205.

Kato, K., Adachi, K. (2000) Wear mechanisms, In: Bhushan, B. (ed.), Modern Tribology Handbook. CRC Press, Boca Raton, Florida, 273–300.

Katz, O., Reches, Z. E. and Baer, G. (2003) *Faults and their associated host rock deformation: Part I. Structure of small faults in a quartz–syenite body, southern Israel*, J. Struct. Geol., *25*, 1675–1689.

Kolmogorov, A.N., Petrovskii, I.G., and Piscounov, N.S. (1937) *A study of the diffusion equation with increase in the amount of substance, and its application to a biological problem*, Bull. Moscow Univ., Math. Mech. *1*, 1–25. Translated by V.M. Volosov in V.M. Tikhomirov, editor, Selected Works of A. N.

Krajcinovic, D. (1996) Damage Mechanics, Amsterdam, Elsevier. 774 p.

Kroner, E., (1968) *Elasticity theory of materials with long-range cohesive force*. Int. J. Solids Struct., *3*, 731–742.

Lemaitre, J. (1996) A Course on Damage Mechanics, Springer-Verlag, Berlin.

Levy, A. V., and Jee, N. (1988) *Unlubricated sliding wear of ceramic materials*, Wear, *121*, 363–380.

Lifshitz, E.M. and Pitaevskii, L.P. (1981) Physical Kinetics, Course of Theoretical Physics, L.D. Landau and E.M. Lifshitz, Vol. 10, Elsevier, 452 p.

Lockner, D.A., Morrow, C., Moore, D. and Hickman, S. (2011) *Low strength of deep San Andreas fault gouge from SAFOD core*, Nature, 472, p. doi:10.1038/nature09927.

Lockner, D.A., Recher, Z., Moore, D.E. (1992) Microcrack interaction leading to shear fracture. In Proc. 33rd U.S. Symposium on Rock Mechanics (ed. W. Wawersik), A.A. Balkema Rotterdam.

Lu, K., Brodsky, E.E., and Kavehpour, H.P. (2007) *Shear-weakening of the transitional regime for granular flow*, J. Fluid Mech., *587*, 347–372.

Lyakhovsky, V., Ben-Zion, Y. and Agnon, A., (2005) *A visco-elastic damage rheology and rate- and state-dependent friction*. Geophys. J. Int. *161*, 179–190.

Lyakhovsky, V., and Ben-Zion Y., (2014a), *Damage-Breakage rheology model and solid-granular transition near brittle instability*, J. Mech. Phys. Solids, *64*, 184–197.

Lyakhovsky V. and Ben-Zion Y. (2014b) *Continuum damage-breakage model for faulting accounting for solid-granular transition*, Pure Appl. Geophys. (this volume).

Lyakhovsky V., Hamiel, Y. and Ben-Zion, Y. (2011) *A non-local visco-elastic damage model and dynamic fracturing*. J. Mech. Phys. Solids, *59*, 1752–1776. doi:10.1016/j.jmps.2011.05.016.

Lyakhovsky, V., Ben-Zion, Y., and Agnon, A. (1997) *Distributed damage, faulting, and friction*, J. Geophys. Res., *102*, 27635–27649.

Ma, S. K. (2000), Modern theory of critical phenomena, Westview press, 561 p.

Marone, C., (1998), *Laboratory-derived friction laws and their application to seismic faulting*, Annu. Rev. Earth Planet. Sci., *26*, 643–649.

Muhuri, S.K., Dewers, T.A., Scott, T.E., and Reches, Z. (2003) *Interseismic fault strengthening and earthquake-slip stability: Friction or cohesion?* Geology, *31*(10), 881–884.

Murray, J. D. (2002) Mathematical Biology: I. An Introduction, 3rd ed., Springer, 551 p.

Newman W.I. and Phoenix, S.L. (2001) *Time-dependent fiber bundles with local load sharing*, Phys. Rev. E., *63*(2), 021507, doi:10.1103/PhysRevE.63.021507.

Nielsen, S., Di Toro, G. and Griffith, W.A. (2010), *Friction and roughness of a melting rock surface*. Geophys. J. Int. *182*, 299–310.

Nolen, J., Roquejoffre, J.M., Ryzhik, L. and Zlatoš, A. (2012) *Existence and non-existence of Fisher-KPP transition fronts*, Arch. Rational Mech. Anal., *203*, 217–246, doi:10.1007/s00205-011-0449-4.

Onsager, L., (1931), *Reciprocal relations in irreversible processes*. Phys. Rev., *37*, 405–416.

Paterson, M.S. and Wong, T.-F. (2005) Experimental Rock Deformation—The Brittle Field. Berlin, Heidelberg, New York: Springer-Verlag, 348 pp.

Petit, J.P. (1987) *Criteria for the sense of movement on fault surfaces in brittle rocks*, J. Struct. Geol., *9*, 597–608.

Power, W.L., Tullis, T.E. and Weeks, J.D. (1988) *Roughness and wear during brittle faulting*, J. Geophys. Res. *93*, 15268–15278.

Queener, C.A., Smith, T.C., and Mitchell, W.L. (1965) *Transient wear of machine parts*, Wear, *8*, 391–400.

Rabinowicz, E., Dunn, L.A., and Russell, P.G. (1961) *A study of abrasive wear under three-body conditions*, Wear, *4*, 345–355.

Rabotnov, Y.N. (1959) A mechanism of a long time failure, in: Creep problems in structural members, 5–7, USSR Academy of Sci. Publ., Moscow.

Rabotnov, Y.N. (1988) *Mechanics of Deformable Solids, Moscow*, Science, 712 p.

Reches, Z. and Lockner, D.A., (1994) *Nucleation and growth of faults in brittle rocks*. J. Geophys. Res., *99*, 18159–18173, doi:10.1029/94JB00115.

Reches, Z., and Lockner, D.A. (2010) *Fault weakening and earthquake instability by powder lubrication*, Nature, *467*, 452–456, doi:10.1038/nature09348.

Ricard, Y. and Bercovici, D. (2009) *A continuum theory of grain-size evolution and damage*, J. Geophys. Res., *114*. doi:10.1029/2007JB005491.

Robinson, E.L. (1952) *Effect of temperature variation on the long-term rupture strength of steels*, Trans. Am. Soc. Mech. Eng., *174*, 777–781.

Sagy, A. and Brodsky, E.E. (2009) *Geometric and rheological asperities in an exposed fault zone*, J. Geophys. Res. *114*, B02301. doi:10.1029/2008JB005701.

Sammis, C., Lockner, D., Reches, Z., 2011. *The role of adsorbed water on the friction of a layer of submicron particles*. Pure Appl. Geophys. *168*, 2325–2334.

Scholz, C.H. (1987) *Wear and gouge formation in brittle faulting*, Geology, *15*, 493–495.

Scholz, C.H., (2002) The Mechanics of Earthquakes and Faulting, 2nd ed. Cambridge University Press, 471 p.

Shcherbakov, R. and Turcotte, D.L. (2003) *Damage and self-similarity in fracture*, Theor. Appl. Fracture Mech., *39*, 245–258.

Shipton, Z.K., Evans, J.P., Abercrombie, R.E., and Brodsky, E.E. (2006) The missing sinks: slip localization in faults, damage zones, and the seismic energy budget, In: Abercrombie, R. (eds.) Earthquakes: Radiated Energy and the Physics of Faulting, 217–222. Washington, DC.

Sibson, R.H. (1977) *Fault rocks and fault mechanisms*. J. Geol. Soc. *133*, 191–213.

Turcotte, D.L., Newman, W.I., and Shcherbakov, R. (2003) *Micro and macroscopic models of rock fracture*, Geophys. J. Int., *152*, 718–728.

Wang, W. and Scholz, C.H. (1994) *Wear processes during frictional sliding of rock: a theoretical and experimental study*. J. Geophys. Res., *99*, 6789–6799.

Wibberley, C.A., Yielding, G., and Di Toro, G. (2008) *Recent advances in the understanding of fault zone internal structure: A review*. Geol. Soc., London, Special Publ., *299*, 5–33.

Wilson, B.T., Dewers, T., Reches, T. and Brune, J.N. (2005) *Particle size and energetics of gouge from earthquake rupture zones*. Nature, *434*, 749–752.

Zang, A., Wagner, F., Stanchits, S., Janssen, C. and Dresen, G., 2000. *Fracture process zone in granite*, J. Geophys. Res., *105*, 23651–23661.

(Received August 28, 2013, revised January 29, 2014, accepted January 30, 2014, Published online February 26, 2014)